

Molecular-Level Engineering of Adhesion in Carbon Nanomaterial Interfaces

Michael R. Roenbeck,[†] Al'ona Furmanchuk,[‡] Zhi An,[‡] Jeffrey T. Paci,^{‡,§} Xiaoding Wei,^{†,§} SonBinh T. Nguyen,^{*,‡} George C. Schatz,^{*,‡} and Horacio D. Espinosa^{*,†,§}

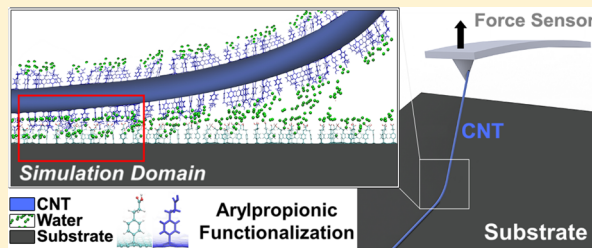
[†]Department of Mechanical Engineering, [‡]Department of Chemistry, and [§]Theoretical and Applied Mechanics Program, Northwestern University, 2145 Sheridan Road, Evanston, Illinois 60208, United States

[‡]Department of Chemistry, University of Victoria, British Columbia V8W 3V6, Canada

Supporting Information

ABSTRACT: Weak interfilament van der Waals interactions are potentially a significant roadblock in the development of carbon nanotube- (CNT-) and graphene-based nanocomposites. Chemical functionalization is envisioned as a means of introducing stronger intermolecular interactions at nanoscale interfaces, which in turn could enhance composite strength. This paper reports measurements of the adhesive energy of CNT–graphite interfaces functionalized with various coverages of arylpropionic acid. Peeling experiments conducted *in situ* in a scanning electron microscope show significantly larger adhesive energies compared to previously obtained measurements for unfunctionalized surfaces (Roenbeck et al. *ACS Nano* 2014, 8 (1), 124–138). Surprisingly, however, the adhesive energies are significantly higher when both surfaces have intermediate coverages than when one surface is densely functionalized. Atomistic simulations reveal a novel functional group interdiffusion mechanism, which arises for intermediate coverages in the presence of water. This interdiffusion is not observed when one surface is densely functionalized, resulting in energy trends that correlate with those observed in experiments. This unique intermolecular interaction mechanism, revealed through the integrated experimental–computational approach presented here, provides significant insights for use in the development of next-generation nanocomposites.

KEYWORDS: Carbon-based nanomaterials, chemical functionalization, adhesive energy, surface energy, *in situ* SEM testing, atomistic simulations



Carbon nanomaterials such as carbon nanotubes (CNTs) and graphene exhibit extraordinary mechanical stiffness (~ 1 TPa) and strength (~ 100 GPa), which makes them ideal candidates as strong, lightweight, load-bearing filaments within next-generation composites.^{1–7} However, while individual CNTs and monolayer graphene sheets are robust, interactions between individual filaments are weak by comparison.^{8–10} The significant disparity in strengths stems from the molecular bonds that govern these interactions: while individual CNT and graphene filaments are held together by sp^2 bonds, which are strong, they adhere to each other through van der Waals (vdWs) interactions, which are weak.⁸ It is thus not surprising that the mechanical properties of composites derived from carbon nanomaterials fall short of the properties of their constituents.^{11–15} van der Waals-driven interfilament interactions thus appear to present a significant bottleneck in the design of carbon nanomaterial composites.

To address this challenge, developing ways to effectively transfer load between nanoscale constituents is a necessary prerequisite for designing strong, lightweight composites from these materials. Many studies have taken a top-down approach to this problem by developing and exploring behaviors of different composites. For instance, integrating soft, extensible

polymers with CNTs in macroscopic CNT yarns has yielded significant insights. Espinosa, Nguyen, and co-workers demonstrated that controlled introduction of poly(vinyl alcohol) into CNT yarns spun from mats can yield increases in stiffness and energy to failure.¹³ Vilatela et al. showed, through *in situ* Raman characterization of CNT yarns undergoing tensile tests, that poly(methyl methacrylate) improves load transfer among CNTs when compared to pristine CNT yarns.¹⁶ Beyond the introduction of polymer alone, chemical functionalization of carbon nanomaterials has also been envisioned as a means of enhancing interfilament interactions.¹⁷ Indeed, significant efforts have been undertaken to investigate the properties of composites with functionalized carbon nanotubes and graphene.^{18–24} While top-down studies of macroscopic composites provide insight into the improvements in performance upon inclusion of carbon nanomaterials, it is difficult to compare the properties of composites among differences in studies to guide materials design due to different processing

Received: March 13, 2015

Revised: May 29, 2015

Published: June 11, 2015

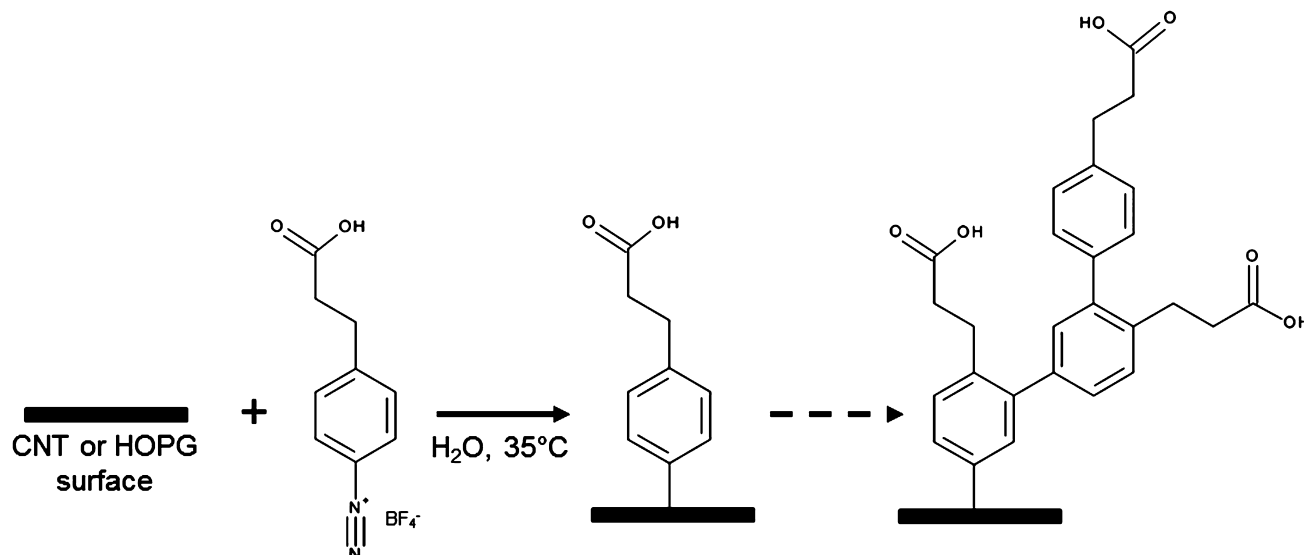


Figure 1. Functionalization of the graphitic surfaces of MWCNTs and HOPG is carried out using diazonium salts.

conditions, system sizes, and other factors. Though interactions between adjacent filaments certainly contribute to mechanical behavior, other global design factors, such as filament alignment^{14,25–27} and porosity, also play critical roles in performance.^{14,25–27} Consequently, it is difficult to isolate improvements in interfilament interactions based on top-down studies of composites alone.

To complement findings obtained through macroscale studies, an alternative approach is to isolate nanoscale filaments and explore ways to make their interfaces more adhesive. Many types of chemical functionalization have been proposed in the literature to introduce new interfacial bonding mechanisms that modify interfilament interactions.¹⁷ Among these mechanisms, hydrogen bonding has proven to be particularly promising, as hydrogen bonds are approximately one order of magnitude stronger than vdW interactions.²⁸ Effective functionalization of interfaces with structures that can participate in intersurface hydrogen bonding brings the possibility of continuously reforming interfacial contacts.²⁹ This is especially advantageous when attempting to prevent filaments from sliding or separating. Indeed, the strength and toughness of dragline spider silk, which utilizes hydrogen bonding to bridge beta-sheet filaments, make it a convincing natural example of the capabilities of hydrogen bonding.^{29–31} Human bones, at the smallest scale of their hierarchical structure, also rely on hydrogen-bond breaking and reformation to enable large deformation of tropocollagen fibrils,³² thus dissipating significant energy prior to fracture.^{27,31,33,34} Considering the high strength and toughness of natural materials that take advantage of hydrogen bonding, it is of great scientific interest to further explore nanoscale behavior of interfaces that utilize this bonding mechanism.

Here, we explore the effect of chemical functionalization on the adhesion of nanoscale interfaces between multiwalled carbon nanotubes (MWCNTs) and highly ordered pyrolytic graphite (HOPG). We introduce aryl-propionic acid groups (Figure 1) onto these materials to enable hydrogen-bonding mechanisms at the interface. We experimentally quantify the adhesive energy, the reversible work of creating the exposed surfaces (i.e., twice the surface energy), as well as the irreversible work of separation during peeling by peeling

MWCNTs from HOPG *in situ* in a scanning electron microscope.³⁵ We compare these results with our previous peeling study of bare nanoscale graphitic interfaces³⁶ to explore the possibility of improvements in adhesion associated with chemical functionalization. We also develop atomistic models to explain changes in surface energy (γ) and adhesive energy ($2\gamma + \text{dissipated energy}$) and provide insights into deformation mechanisms at the interfaces between these materials. Our integrated computational–experimental approach comprises a strategy for screening potentially useful functionalizations through computational models and then verifying the adhesion predictions experimentally, enabling the bottom-up design of strong, lightweight composites that effectively leverage the exceptional mechanical properties of carbon nanomaterials.

Materials Synthesis and Characterization. Arylpropionic-acid-functionalized MWCNTs and HOPG were prepared using diazonium chemistry (Figure 1, see the Supporting Information for details).^{37–39} Arylpropionic acid was selected because it is hypothesized to exhibit suitable coverage and flexibility for introducing hydrogen bonds at the interface between functionalized MWCNTs and HOPG. The moderate flexibility of the propionic acid chain may allow for a variety of possible conformations in which hydrogen bonds can form between opposing surfaces (intersurface). Longer chains with more flexibility could lead to the terminal carboxylic acid moieties bonding with each other within the same surface (intrasurface) or folding onto the surface, exposing the nonpolar alkylic part of the structure rather than the terminal groups that were designed to yield hydrogen bonds.^{40,41} (In our system such configurations are expected to be limited by the rigid phenyl part at the base of each propionic group, which separates polar moieties and restricts intrasurface bonding.)

The coverage formed by phenyl-based groups during application of diazonium chemistry to graphitic surfaces is expected to be random, as well-ordered functionalization has been shown to be impossible for graphitic materials.^{42–44} In light of these factors, the functional groups used in this study should effectively introduce well-distributed hydrogen bonds at these nanoscale interfaces. Recent studies suggest that covalently bound oligomers⁴⁵ and physisorbed oligomers⁴⁶ may also be present on HOPG surfaces prepared with

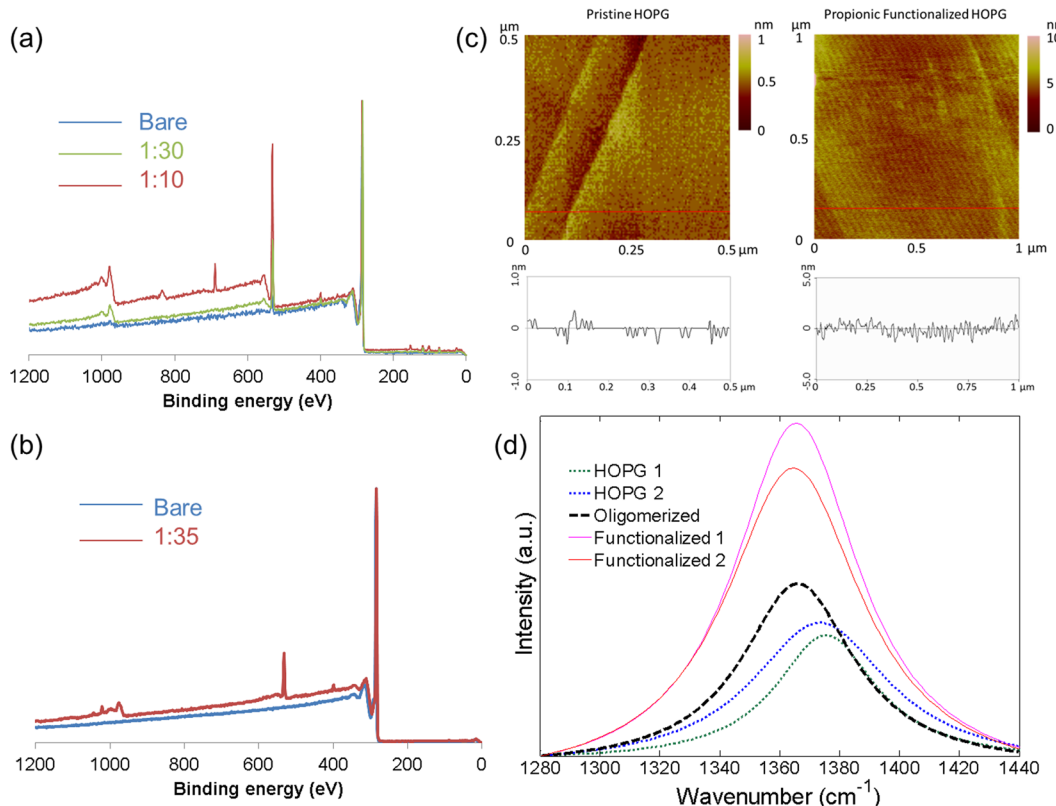


Figure 2. Characterization data for MWCNTs and HOPG. (a) XPS survey scans of bare and functionalized MWCNTs. (b) XPS survey scans of bare and functionalized HOPG. Spectra are normalized by the height of the C 1s peak. (c) Noncontact mode AFM topography scans of pristine and functionalized HOPG. Height profiles of representative line scans are shown below each image. (d) Lorentzian fits of the D peaks for bare, oligomerized (control), and propionic acid-functionalized HOPG.

diazonium chemistry. Additional details regarding these findings and their implications for experimental measurements are included in the Discussion section.

Functionalization density was estimated using X-ray photoelectron spectroscopy (XPS) (see Figure 2a,b) after subtracting contributions from the oxygen of strongly adsorbed water, the carbon from the underlying layers of the MWCNT and HOPG, the oxygen from the underlying alumina filter membrane, and small amounts of oxygen present on the bare tubes (see the Supporting Information for details). Our heavily functionalized ones had a functionalization density of approximately 1 in 10 surface carbon atoms, while the moderately functionalized tubes had a density of approximately 1 in 30 carbons. Our HOPG had a functionalization density of approximately 1 in 35 surface carbons. In subsequent sections, we refer to these ratios of one functional group per N surface carbon atoms as 1:N (e.g., 1:10, 1:30, and 1:35).

Raman spectroscopy was used to determine whether or not functional groups were covalently bound to the graphite surface. In addition to a prominent G-band ($\sim 1580 \text{ cm}^{-1}$) associated with in-plane sp^2 optical vibrations, a characteristic D peak ($\sim 1350 \text{ cm}^{-1}$) is associated with disordered carbon structures.^{47–49} Studies have ascribed the presence or increase of a D peak to sp^3 bonding induced by aryl group functionalization.^{42,49–52} While functionalizations expected to be physisorbed on the surface of graphene have also exhibited increased D peaks compared to pristine graphene,^{46,53,54} the magnitude of these peaks is lower than that of covalently functionalized graphene.⁴² It is thus hypothesized that the same

trend would hold for HOPG with a functionalized top surface such as in this study.

In accordance with the literature,⁴² we prepared control samples with oligomerized functional groups that are expected to be physisorbed rather than covalently bound to the surface (see the Supporting Information). Fits of the resulting D peaks (see Methods) are plotted in Figure 2, panel d. While the oligomerized control sample exhibited a slight increase (~30%) in the integrated area of the peak compared to the pristine sample, the increase in the peaks of the functionalized sample was over 140%. Since the relative sizes of these peaks correspond well with literature reports,⁴² these results suggest that covalently bound functional groups are present on the surface of the HOPG used in testing. (Note that the result is equally consistent with the covalent binding of monomers or oligomers.)

An atomic force microscope (AFM) was used in tapping mode to examine the smoothness of the functionalized HOPG surfaces. Figure 2, panel c shows the topographies of pristine and functionalized graphite. The pristine samples appeared atomically smooth, although steps of single graphene layers, presumably due to the cleavage, were observed. The roughness was approximately 0.1 nm.³⁶ The functionalized surfaces were found to be rougher, with the scan over a $1 \times 1 \mu\text{m}^2$ area yielding a uniform roughness of approximately 0.7–0.8 nm. This suggests the functionalization was distributed evenly. The aforementioned step features remained after the functionalization, and they are believed to contribute to the scatter of the peeling data. However, since the CNT diameters (25–27 nm) are much larger than the measured roughness, the function-

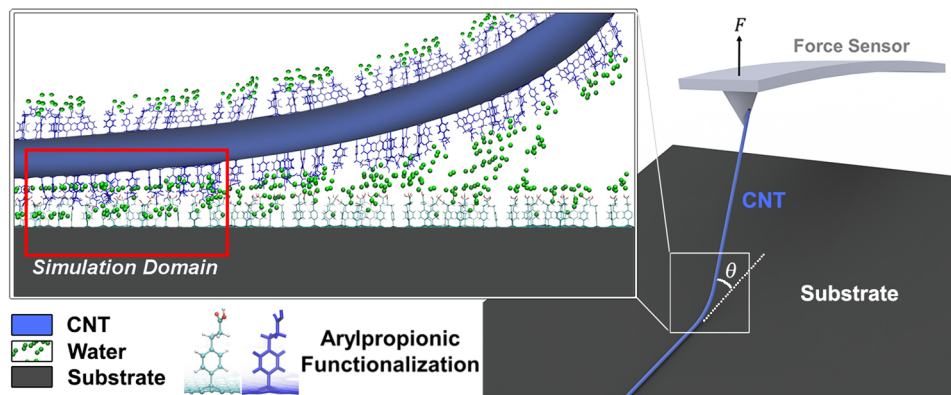


Figure 3. Experimental setup and simulation domain. In the experiments, an AFM cantilever (force sensor) with an attached CNT is brought into contact with an HOPG substrate within an SEM. As the substrate is pulled away, the force F on the CNT and angle θ with respect to the substrate are monitored. In the simulations, graphene bilayers functionalized with propionic groups are used to explore the geometries and energetics associated with peeling.

Table 1. Experimental Measurements and Calculated Adhesive Energies for Functionalized MWCNT–HOPG Interfaces

functionalization level	tube no.	peel angle, θ [°]	force, F [nN]	outer diameter [nm]	number of walls	collapsed width, w_C [nm]	flattened width, w_F [nm]	collapsed adhesive energy, R_C [$J\ m^{-2}$]	flattened adhesive energy, R_F [$J\ m^{-2}$]
1:10 on 1:35	1	54	46	25	31	14.8	8.0	1.29 ± 0.27	2.37 ± 0.80
1:10 on 1:35	1	52	59	25	31	14.8	8.0	1.56 ± 0.33	2.88 ± 0.96
1:10 on 1:35	2	40	59	26	31	14.9	8.1	0.92 ± 0.18	1.69 ± 0.55
1:10 on 1:35	2	42	94	26	31	14.9	8.1	1.59 ± 0.31	2.94 ± 0.96
1:10 on 1:35	2	42	99	26	31	14.9	8.1	1.71 ± 0.34	3.16 ± 1.03
1:10 on 1:35	2	45	108	26	31	14.9	8.1	2.13 ± 0.42	3.93 ± 1.28
1:10 on 1:35	2	40	114	26	31	14.9	8.1	1.77 ± 0.36	3.28 ± 1.08
1:30 on 1:35	1	54	83	26	31	14.9	8.0	2.31 ± 0.45	4.28 ± 1.39
1:30 on 1:35	1	58	81	26	31	14.9	8.0	2.56 ± 0.49	4.72 ± 1.53
1:30 on 1:35	1	55	96	26	31	14.9	8.0	2.72 ± 0.52	5.03 ± 1.63
1:30 on 1:35	1	54	95	26	31	14.9	8.0	2.63 ± 0.51	4.85 ± 1.57
1:30 on 1:35	2	50	100	27	33	15.1	8.2	2.40 ± 0.46	4.44 ± 1.42
1:30 on 1:35	2	44	141	27	33	15.1	8.2	2.65 ± 0.51	4.94 ± 1.58

alized graphite can be approximated as smooth and flat for the experimental analysis and the modeling.

In Situ Scanning Electron Microscope (SEM) Testing.

In situ SEM testing was carried out using a methodology previously employed by us for MWCNT–graphene and MWCNT–HOPG interfaces.³⁶ A schematic representation of the experimental setup is shown in Figure 3. Briefly, an AFM cantilever (of known stiffness) extending from a nanomanipulator was brought into contact with a MWCNT in situ in a SEM. The ~5 μm-long CNT was cut using a focused electron beam and welded to the cantilever via amorphous carbon deposition. The tube was then brought into contact with the graphite substrate attached to the SEM stage. Finally, by retracting the stage, the tube detached from the substrate through successive small peels (approximately 100 nm in length). The AFM cantilever deflection and tube profile were recorded at regular intervals to facilitate the evaluation of the applied force and pulling angle at the onset of peeling.

The adhesive energies were estimated using an analysis developed by Kendall.⁵⁵ Kendall's formula, which assumes an energy balance and no dissipation outside the vicinity where the actual separation occurs (i.e., only local dissipation), states that:

$$F(1 - \cos(\theta)) = R w - \frac{F^2}{2\pi E dt} \quad (1)$$

where F is the applied force, θ is the peeling angle, R is the adhesive energy, w is the effective contact width, E is the elastic modulus of the CNT (taken to be 1 TPa^{3,4}), d is the diameter, and t is the thickness of the outermost wall (which is expected to bear the majority of the load⁴). The term on the left corresponds to work done by the cantilever, while the first and second terms on the right denote the energy required to create new surfaces and the elastic strain energy of the tube, respectively. Rearranging eq 1 affords the adhesive energy R as:

$$R = \frac{1}{w} \left\{ F(1 - \cos(\theta)) + \frac{F^2}{2\pi E dt} \right\} \quad (2)$$

As noted by Kendall,⁵⁵ the adhesive energy R measured experimentally includes the work of adhesion as well as local dissipation. If nonlocal dissipation (e.g., tube or graphite plasticity) is important in a system, Kendall-based estimates of the adhesive energy will be too high. In the ideal limit where free surfaces are created without dissipation, the adhesive energy can be equated to the work of adhesion, or twice the surface energy (i.e., 2γ). Additional discussion regarding the assumptions associated with applying Kendall's model is included in the Supporting Information.

Atomistic Simulations. A schematic of a representative system studied with atomistic simulations is shown in Figure 3. Two 3 nm × 3 nm graphene bilayers were prepared with

periodic boundary conditions applied in all three dimensions. Vacuum regions of 3 nm were added above and below the outermost graphene layers. The inner layers were randomly functionalized with arylpropionic monomers with high (1:11) and moderate (1:35) coverages to match the experimental coverages as closely as possible, while the outermost graphene layers were added to stabilize the inner surfaces (see Methods). Simulations were performed using the all-atom optimized potentials for liquid simulations (OPLS-AA)^{56,57} as implemented in Tinker 6.3.⁵⁸ Systems were analyzed without water (representing ultrahigh vacuum conditions) and with two simple point charge (SPC) water molecules per functional group (corresponding to $\sim 1 \times 10^{-5}$ Torr pressure in the SEM). Molecular mechanics (MM) was used for the stepwise compression or opening of interfaces. To confirm that the interface geometries predicted by MM were realistic, systems were also equilibrated at 300 K using molecular dynamics (MD) with an NVT ensemble until conservation of energy was established. Relative energy values reflect the energy required to open the equilibrated interfaces, equivalent to twice the surface energy (2γ). Additional information regarding simulations is provided in the Methods section and Supporting Information.

Results and Discussion. Experimental Adhesive Energy.

To evaluate the adhesive energies of arylpropionic-functionalized interfaces, two CNTs with 1:10 functionalization and two CNTs with 1:30 functionalization were peeled from 1:35 functionalized HOPG substrates. As noted earlier, multiple small peels were induced during a given test, which enabled several data points to be extracted per test. Detailed experimental results, including forces and peeling angles for each peel with functionalized materials, are reported in Table 1.

It is important to contextualize and standardize the energy values obtained with these functionalized surfaces with respect to (i) previously obtained data for bare MWCNT-graphite interfaces and (ii) atomistic simulation predictions. For this purpose, we focus on comparing adhesive energy results assuming a flattened MWCNT configuration. The term “flattened” is derived from our previous work³⁶ where it was determined that MWCNTs can either be flattened or collapsed on a surface depending on nanotube diameter and number of walls. This influences the contact width that is utilized in the Kendall analysis, leading to ambiguity in the adhesive energy values. For completeness, contact widths and adhesive energies are reported using both conformation types in Table 1 (with subscripts “C” and “F” denoting collapsed and flattened, respectively). However, while both conformations are possible, MWCNTs with the diameters and numbers of walls reported in Table 1 are not expected to achieve a collapsed configuration, so adhesive energies assuming a flattened configuration are the most appropriate standard.³⁶ These results for functionalized interfaces, as well as data for the bare interfaces previously studied by us,³⁶ are shown in Figure 4. (We note that the amount of flattening or other factors, such as graphitic deposits,⁵⁹ that increase contact area would lead to smaller adhesive energies than are reported.)

The eight data points reported in ref 36 for bare graphite and graphene yielded an average adhesive energy (taken as twice the γ values reported) of 0.73 J m^{-2} with a standard deviation of 0.30 J m^{-2} . By comparison, the 1:10 on 1:35 tube-HOPG interfaces exhibited an average adhesive energy of 2.89 J m^{-2} with a standard deviation of 0.71 J m^{-2} . Finally, the average adhesive energy of the 1:30 on 1:35 interfaces was 4.71 J m^{-2} with a standard deviation of 0.29 J m^{-2} . Unpaired t tests

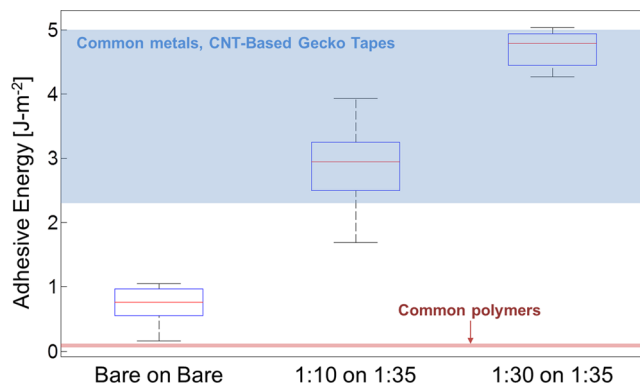


Figure 4. Experimental adhesive energies for bare–bare, 1:10 on 1:35, and 1:30 on 1:35 surfaces. The bare–bare data were taken from ref 36. For comparison, adhesive energies reported for common metals and CNT-based gecko tapes (adhered to various substrates) as well as adhesion energies for common polymers are included.^{28,69–71}

between each pair of data sets indicate that there is a statistically significant difference ($p < 0.05$) between each of the mean values.

The role of dissipation in these adhesive energy measurements merits further discussion. In all cases, the energy values measured are small enough and the tubes and graphite are strong enough that we expect no significant nonlocal dissipation. For bare CNT–graphene/graphite interfaces, the adhesive energy measured was close to twice the surface energy of graphite reported in the literature, suggesting that energy dissipation is not significant when separating those interfaces.^{36,60–62} However, the adhesive energy measured for arylpropionic-functionalized interfaces cannot be compared with literature values; this is a novel system. Atomistic simulations were thus carried out to predict the surface energy of these interfaces as a function of coverage and, through comparison with experiments, assess the degree to which local dissipation contributes to adhesive energy measurements. In addition, the nature of interfacial interactions predicted via simulations can elucidate the mechanisms that underlie a surprise experimental finding: intermediate coverages, not high coverages, yield the highest adhesive energies.

Theoretical Surface Energy. One may expect that hydrogen bonds would be the dominant factor defining the adhesive properties of these surfaces. Therefore, it would seem intuitive that highly functionalized surfaces would exhibit stronger adhesion than those with moderate functionalization, as the former have more potential for intersurface bonds to form. Indeed, atomistic simulations in ultrahigh vacuum (UHV) conditions (see the Supporting Information, especially Figure S8) support this hypothesis. Moderately functionalized surfaces in UHV tend to have weaker adhesion due to a smaller number of intersurface hydrogen bonds compared to more highly functionalized interfaces.

However, while the simulations under UHV conditions serve as a useful test case, ambient water is expected to play a critical role in the behavior of arylpropionic acid functionalized interfaces. As shown in studies of materials such as spider silk and aramid single fibers, the presence of water can significantly alter the performance of interfaces involving hydrogen bonding.^{63–65} Our XPS data (see the Supporting Information) suggest that ambient water content in our in situ SEM peeling experiments could be as low as two water molecules per

functional group, so we added this much water to our models as a first approximation.

The surface structures associated with two choices of functionalized surfaces are presented in Figure 5. Water

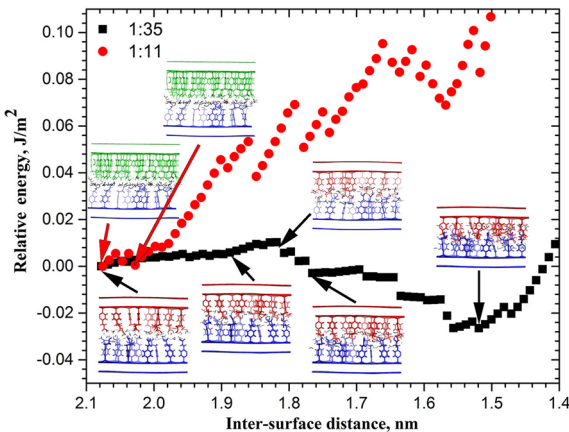


Figure 5. Energy profiles for the stepwise compression of interfaces formed by 1:35 on 1:35 (black squares) and 1:11 on 1:35 (red dots) functionalized surfaces in the presence of water. Insets are illustrations of configurations of interfaces at particular steps.

molecules cannot penetrate the densely packed functional groups of the 1:11 surfaces, so they mediate hydrogen-bond interactions with this surface (see the insets in Figure 5). The overall structure of the 1:11 on 1:35 interface is therefore similar to what was found in the absence of water for the same coverage. In contrast, for moderate functionalization (1:35 on 1:35), some water molecules move into gaps between groups. The rest form hydrogen bonds with carboxylic groups within the polar parts of the interface region and with other water molecules. Compression of these surfaces leads to an interdiffused structure of lower energy, with little or no barrier for formation of a structure with a 1.5 nm separation.

While the picture in Figure 5 is qualitatively similar to that in Figure S6 in the Supporting Information, we were unable to generate well-defined minimum energy structures for the energy profiles shown in Figure 5 using the stepwise compression procedure employed in the latter figure. This is because the energy minimization process for Figure 5 leads to many local minima corresponding to embedded water cluster structures of different sizes. As an alternative, we selected several interface configurations from along the compression path (see the insets in Figure 5) and equilibrated them at 300 K. Examination of the resulting structures revealed that for the 1:11 on 1:35 structure (Figure 6, right panels), the water molecules are always localized near the carboxylic groups. For the 1:35 on 1:35 interface (Figure 6, left panels) there are isolated water clusters and alkyl–alkyl interactions that stabilize the interacting surfaces. Interactions between two heavily functionalized surfaces such as 1:11 on 1:11 (not shown in Figure 6) showed no intersurface hydrogen bonds between functional groups; instead, water links carboxylic groups bound to opposing surfaces.

Deep interdiffusion of the arylpropionic acid functional groups layers was only observed if neither of the interacting surfaces was heavily functionalized. For deep interdiffusion, the surface restructuring was complex, even more so than in the water-free cases. Peeling (or shearing) of such interfaces should require more force than would be expected for surfaces without

interdiffusion due to the effective segregation of hydrophobic and hydrophilic regions as well as a relatively high area of interacting surface. For example, repulsive interactions that occur when a hydrophilic region is moved into a hydrophobic area can result in resistance to pulling the interdiffused layers apart, thereby acting as a net attraction. This is in contrast to what happens for surfaces that do not diffuse into one another, in which case only hydrophilic interactions (hydrogen bonds) are attractive (Figure 6).

We selected several equilibrium configurations (at 300 K) to provide a statistically meaningful evaluation of the possible interaction mechanisms activated during the peeling tests. The resulting energy-displacement curves, when averaged over multiple stepwise peeling procedures (Figure 7), provide insights into these mechanisms. To provide a reference point and understand trends, we started from identically functionalized interfaces in vacuum (no water). Under these conditions, the 1:35 on 1:11 interfaces exhibited a higher relative energy ($\sim 0.08 \text{ J/m}^2$) than the 1:35 on 1:35 systems ($\sim 0.04 \text{ J/m}^2$) (see Figure 7a,b). This is due to the aforementioned correlation between the surface energy and the number of intersurface hydrogen bonds. However, structural transformations in interdiffused arylpropionic acid layers mean there is an additional step in the opening mechanism. This step results in extra energy relaxation that is sufficiently effective to create an energy barrier of $\sim 0.14 \text{ J/m}^2$ for the 1:35 on 1:35 systems in the presence of water. Interfaces where one or both surfaces are heavily functionalized only operate via hydrogen-bond interactions. Therefore, the adhesion energies are lower ($\sim 0.11 \text{ J/m}^2$ for 1:11 on 1:35). The fact that the trends in adhesion from simulations that include water match the trends observed experimentally, while those without water do not, highlights the importance of accounting for the role of water in these systems. While this is not as critical for surface interactions governed by vdWs adhesion (e.g., bare graphitic surfaces), the inclusion of water elucidates a unique mechanism—functional group interdiffusion—that is expected to contribute to the enhancements in adhesion observed in experiments.

The arylpropionic acid groups are so sufficiently rigid that they keep the graphene basal planes well separated. As a result, they prevent the surfaces from approaching the vdWs minimum associated with graphite ($\sim 0.34 \text{ nm}$), which means that the vdWs interactions that are present are much weaker than in the bare case. In addition, the intersurface hydrogen bonds have too low a density to compensate for the loss of interactions, so even though the hydrogen bonds are stronger, there are fewer of them. We also find that interdiffusion, when it occurs, increases the surface energy by just a small amount compared to an analogous noninterdiffused case. However, we note that interdiffusion probably plays a role in the experiments that are related to what we find. For the 1:35 on 1:35 case, there is the suggestion of an appreciable average force over $\sim 0.3 \text{ nm}$ between 1.5 and 1.8 nm (see Figure 5) that is nearly constant. Noncovalent bonds are broken and new ones formed, which are then broken as the surfaces interdiffuse. This is not the case when atomistically flat surfaces are in contact.

Calculating surface energies accurately is challenging due to, for example, errors in force fields and difficulties with structural models. The most serious problem arises from statistical errors associated with calculating the small difference between two large numbers (i.e., the energy difference between the equilibrium and separated surfaces). The simulations we have

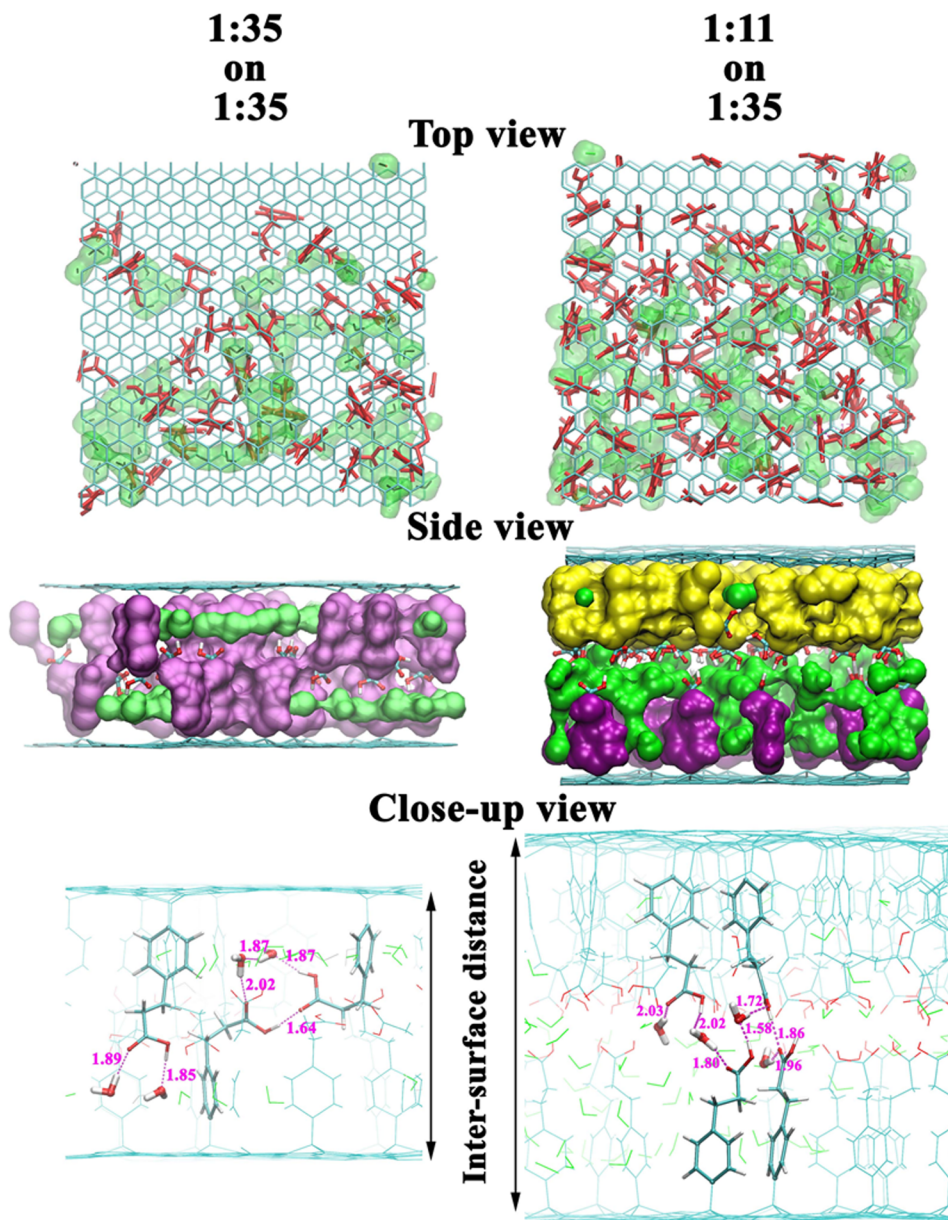


Figure 6. Views of interface regions composed of 1:35 on 1:35 (left) and 1:11 on 1:35 (right) functionalized surfaces. The same snapshot is depicted in each. Top view: Functional groups marked in red and water molecules marked in green lines and clouds. Side view: Purple and yellow clouds represent hydrophobic parts of functional groups for surfaces covered with ratios of 1:35 and 1:11, respectively. Carboxylic groups are shown using stick representations. Close-up view: Representative interactions are shown for each interface. Outer graphene layers are not shown.

performed have necessarily simplified this issue either by doing the calculations at 0 K or by studying models in which the dissociated fragments are assumed rigid rather than being equilibrated. Ultimately, such calculations are not capable of providing quantitative results, although they do provide qualitative insight.

From Surface to Adhesive Energies. While the qualitative trends between simulations and experiments provide critical insights into the adhesion of these interfaces, it is also important to quantitatively compare the results obtained with each method. The theoretically calculated relative energies for the functionalized surfaces are smaller in magnitude than the average experimental values associated with functionalized, and even bare, surfaces.³⁶

In interpreting the theoretical predictions of surface energies, we should point out that the lack of quantitative agreement

between the calculated surface energies and experimentally measured adhesive energies is likely the result of three factors: dissipation, inhomogeneous surfaces, and computational problems with determining relative energies. Of the three, dissipation appears to be the dominant factor. There are many sources of dissipation that might affect the experiments. Interdiffusion takes time, and our MD simulations suggest that 1:35 on 1:35 surfaces interdiffuse in >100 fs (the water cluster rearrangement time). Interdiffusion for the 1:30 on 1:35 surfaces should be much slower than this, as this also requires movement of the arylpropionic acid groups. Peeling in the experiments occurs abruptly; hence, events at the front occur at close to the speed of sound ($\sim 0.1 \text{ \AA/fs}$, i.e., approximately the Rayleigh wave speed), so the time scale for these events is shorter than the interdiffusion time. As a result of the characteristic velocity at the peeling front being faster than

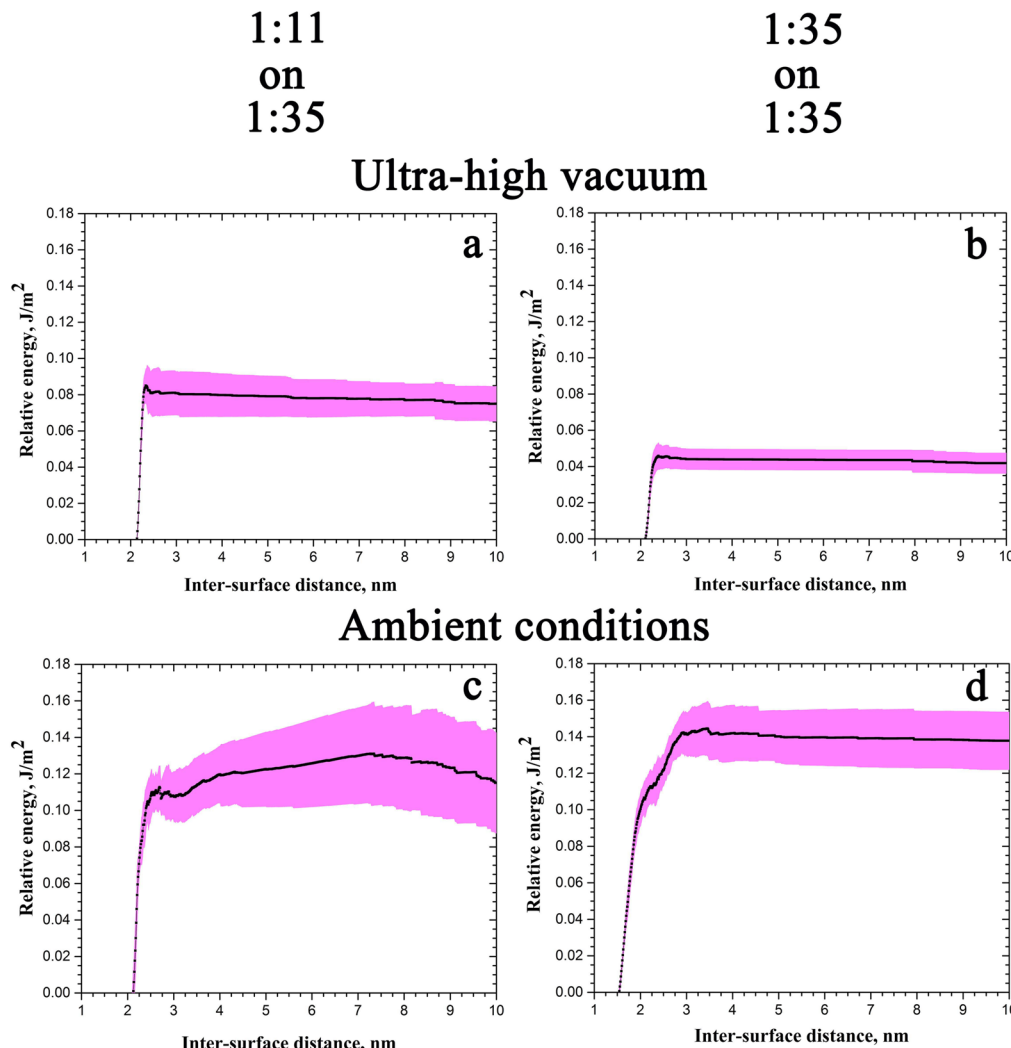


Figure 7. Surface energies from stepwise MM peeling simulations: (a, c) 1:11 on 1:35 and (b, d) 1:35 on 1:35 interfaces. Results in the absence (a, b) and presence (c, d) of water are shown. Averaged curves are depicted in black, and standard deviations of the averages are depicted in pink.

the characteristic interdiffusion velocity, equilibrium will not be maintained during peeling, and irreversible processes (including covalent bond breakage as we discuss next) will lead to adhesive energy measurements much larger than twice the surface energy.⁶⁶ Indeed, the calculated relative energies imply only lower bounds to the energy measured for peeling in experiments.

Ultimately, the significant difference between the surface energy-based predictions and the adhesive energy measured in experiments indicates that irreversible energy dissipation governs the peeling process. On the basis of the energy profiles shown in Figure 5, we believe that the primary dissipation mechanism is the rupture of covalent bonds at the junctions between functional groups and the basal planes of CNTs and HOPG and within the propionic functional groups. For instance, the energy profiles computed for 1:35 on 1:35 surfaces exhibit abrupt changes in energy at intersurface distances of approximately 1.64 and 1.58 nm due to sudden changes of hydrogen-bond distributions. Hence, the average normal stresses acting on the surfaces, given by the derivative of the energy (per unit area) with respect to intersurface distance, are estimated to be as high as 0.6–1.0 GPa. In the simulated 3 nm × 3 nm system (Figure 5, bottom right inset), this

corresponds to a force of up to 9 nN acting over about three intersurface contact points, or ~3 nN per point. This estimate offers an approximate lower bound to the forces that operate at the peeling front in experiments. Since the functional groups on the surfaces are likely to be inhomogeneously distributed, localized forces may be even higher in experiments. In addition, the forces estimated from atomistic simulations correspond to those under infinitely slow separation with idealized geometries. Since the characteristic experimental peeling time is shorter than the characteristic interdiffusion time, additional forces beyond those estimated from Figure 5 will be required to separate interdiffused surfaces in the experiments. Furthermore, for comparison, the strength of sp^3 carbon bonds has been experimentally measured to be as low as ~2.5 nN in some circumstances, which is within range of the approximate lower bound described previously.⁶⁷ Thus, these high transient normal stresses are expected to cause covalent-bond breakage of a substantial number of sp^3 bonds near the joints between functional groups and basal planes and within the propionic groups.

To support this hypothesis, we carried out a first-order estimation of the dissipated energy due to covalent-bond breakage by assuming that two sp^3 bonds per pair of functional

groups ruptured during peeling. Since the dissociation energy of sp^3 bonds is ~ 367 kJ/mol,⁶⁸ the additional energy per unit area required to separate two surfaces with 1:35 functionalization density is approximately 1.3 J m^{-2} . This energy value is on the same order of adhesive energy measurements obtained from our experiments for the functionalized interfaces. Further, covalent-bond breakage is more likely to arise with interdiffused structures and hence with the 1:10 on 1:35 measurements. Therefore, it is reasonable to suggest that local covalent bond breakage appears to be the main energy dissipation mechanism leading to the high adhesive energy values measured in the experiments, which greatly exceed the values predicted through surface energy-based atomistic simulations.

In addition to dissipation, quantitative differences between experimental and theoretical results presented here may arise from inhomogeneous surfaces in the experiments. Recent studies suggest that diazonium chemistry leads to covalently bound oligomers on silicon carbide-supported graphene⁴⁵ and mostly physisorbed oligomers on graphite.⁴⁶ These studies are opposed to other reports that suggest monomers are present on planar surfaces such as HOPG.^{42,50–52} While there is not yet a consensus on the way functional groups adhere to graphite, we cannot rule out the possibility that the arylpropionic groups may also be present as oligomers. Covalent bonding of arylpropionic monomers is expected to occur on the tubes, as the curvatures of ~ 25 nm diameter tubes are greater than those of the ~ 50 nm diameter nanoparticles investigated by Wu et al.⁴⁹ Compared with the systems of monomers studied in our simulations, oligomers would facilitate additional deformation mechanisms and bonding interactions that contribute to adhesion. In addition, while the aforementioned Raman spectroscopy results suggest that some covalent bonding of functional groups is present on the graphite surfaces, any physisorbed material could also be removed during peeling and thus affect energy measurements. Finally, the surfaces are also likely to be fouled by other materials from the atmosphere, such as hydrocarbons, and the tube surfaces are expected to have some amorphous carbon attached.⁵⁹ Their presence should also impact the peeling force, as amorphous carbon is expected to have a different functionalization ratio than the graphitic regions.

Finally, with respect to the field of nanocomposites design, it is important to contextualize these results presented thus far with respect to surface energy and adhesive energy values for other materials reported in the literature. While the aforementioned comparisons with less adhesive interfaces between bare CNTs and graphene/graphite are the most direct, many other materials are also incorporated into composites, so a more complete discussion is warranted. As one example, flexible polymers typically exhibit low surface energies. For instance, the work of adhesion of polystyrene (corresponding to twice the surface energy, γ) has been measured to be $\sim 0.07 \text{ J m}^{-2}$.^{28,69} Other polymers fall in a similar range. Metals, in contrast, are strongly adhesive—for example, the work of adhesion of clean copper (i.e., in the absence of an oxide or surface contaminants) has been shown to be 4 J m^{-2} .^{28,70} This is to be expected in light of the strong, short-range electron exchange interactions that bind metals together.²⁸ Interestingly, the adhesion of macroscopic CNT-based “gecko tapes”, whose structures are inspired by highly adhesive gecko feet, is also within this range. Experimental adhesive energies of CNT tapes on Teflon and mica substrates reported by Ge et al. are 2.2 J m^{-2} and 5 J m^{-2} , respectively.⁷¹

Within these contexts, the adhesive energies measured for both sets of our functionalized materials are well above those of polymers and bare graphitic interfaces, and within the range of other highly adhesive materials. These results accentuate the importance of rational chemical functionalization as a highly promising strategy for enhancing the surface properties of carbon nanomaterials for incorporation into future composites.

There are several additional studies that could provide meaningful insights for adhesion of nanoscale interfaces and its implications for nanocomposites design. At the nanoscale, future studies that aim to complement this work should explore interfilament shearing behavior. While enhanced adhesion leads to enhanced shear, it is important to account for multiple modes of interfilament failure, especially in composites such as CNT yarns, which have great variation in alignment.^{14,72} The effect of functionalization on nanoscale adhesion of rougher graphitic interfaces (e.g., graphene-based interfaces in refs 73 and 74) would also be of significant interest, as interfacial conformations within composites would be expected to vary considerably. Further nanoscale studies could also explore the lower operational limits of this interdiffusion mechanism (i.e., utilizing lower coverages) through detailed simulations and additional experiments. Complementing these bottom-up investigations, additional top-down studies are required to address macroscopic composite features such as porosity and misalignment, which diminish mechanical performance.¹⁴ For example, recent investigations demonstrated that functionalizing MWCNTs⁷⁵ and graphene⁷⁶ with hydrogen atoms leads to improved filament dispersion by interrupting vdWs interactions between agglomerated tubes and sheets. Macroscopically, the improvement in filament distribution within these composites yields superior mechanical properties compared to what has been obtained with traditional dispersion techniques. By developing ways to integrate multiple chemical functionalization steps to first disperse these filaments effectively and, subsequently, improve interfilament adhesion by introducing additional functional groups onto MWCNT outer walls, even further improvement in mechanical performance could be achieved. The interplay between enhanced adhesion and reduced filament strength (resulting from different concentrations of sp^3 bonds on outer surfaces of MWCNTs due to varying coverages), and the resulting impact on composite performance, could also be explored through nanomechanical experiments⁴ and macroscale statistical models.⁷⁷ Ultimately, scaling up these interfaces to the macroscopic level and incorporating them into efficient composite systems remain important engineering challenges for the future.

Concluding Remarks. In summary, we have investigated the effect of arylpropionic acid functionalization on the adhesive properties of nanoscale interfaces through an integrated experimental–computational approach. By peeling functionalized MWCNTs from functionalized HOPG *in situ* in a SEM, we measure high adhesive energies that, counterintuitively, do not scale with the degree of functionalization. We explain this trend through atomistic simulations that account for ambient water present in experiments, which reveal a novel interdiffusion mechanism that is expected to occur at intermediate coverages. When coverage is too high, hydrogen bonding alone is primarily responsible for intersurface adhesion, leading to lower overall surface energy than interdiffused interfaces with intermediate coverages. The qualitative correlation between atomistic predictions and nanoscale experiments suggests that interdiffusion does

contribute to experimental adhesive energy measurements. Quantitative differences in measured adhesion energies and theoretically predicted surface energies reveal that dissipation, arising from covalent-bond breaking, is the primary source of adhesion. Hence, the nanoscale measurements reported in this work support the hypothesis that chemical functionalization of carbon nanomaterial interfaces can significantly improve adhesion at their interfaces. Consequently, these findings provide a unique roadmap for the bottom-up design of nanocomposites that can effectively transfer load between carbon constituents (CNTs, graphene, graphene oxide) and, thus, achieve improved levels of mechanical performance.

Methods. *Raman Spectroscopy.* Raman spectra of the oligomerized sample, pristine HOPG, and the functionalized HOPG used in testing were probed using a Princeton Instrument/Acton Raman microscope (50 \times magnification, 514.5 nm laser, \sim 1.9 cm $^{-1}$ resolution, 100 s per spot). All Raman D peaks were fit with Lorentzian functions.⁴⁸ A full representative spectrum is included in the Supporting Information.

Atomic Force Microscopy. Tapping mode scans were conducted with a Dimension 3100 (Veeco) atomic force microscope. All samples were examined in a sealed chamber under ambient laboratory conditions (\sim 20% relative humidity).

In Situ SEM Experiments. Peeling tests were conducted within an FEI NovaNano 600 SEM. All CNTs were cut using highly focused electron beamline scans (5 kV, 1.8 nA, \geq 300 000 \times magnification for approximately 5 min)⁷⁸ and left for at least 2 h prior to testing to allow the ambient pressure to equilibrate at approximately 1×10^{-5} Torr. In all tests, the HOPG substrate was rotated approximately 30 degrees with respect to the main axis of the AFM cantilever to reduce the likelihood of peels at high angles, which may introduce structural changes to the MWCNTs that affect energy measurements (see the Supporting Information for more details). The diameters of CNTs were estimated by calculating the full width at half-maximum of multiple transverse line scans from high-resolution SEM images. The stiffness of each AFM cantilever (Mikromasch) used in testing was estimated based on dimensions measured in SEM images as well as the elastic modulus reported by the manufacturer. Forces applied by the cantilever on the CNT during peeling were measured through digital image correlation with corrections for inherent cantilever drift. In addition, peeling angles and offset angles were measured directly from SEM images in the frame prior to each peel. For detailed information regarding uncertainty analysis, see ref 36.

Force Field Selection. OPLS-AA has been successfully used to determine densities, enthalpies of vaporization, heat capacities, surface tensions, isothermal compressibilities, volumetric expansion coefficients, and dielectric constants of organic liquids.^{79,80} Studies of organic molecules on the surfaces of water droplets with different water models⁸¹ suggest that density, as well as enthalpy of vaporization, is reproduced well using the OPLS-AA with SPC.⁸² Consequently, this combination is thought to be the most appropriate one currently available for investigating systems such as the arylpropionic-functionalized surfaces used in this study.

Atomistic Simulations. Because the inner walls of MWCNTs are of limited relevance to surface interactions, we restricted the thicknesses of our models. The inner walls provide rigidity and stabilization (via vdWs forces and Pauli repulsion) to the outer walls. Simulations indicated that

functionalized single-graphene layers were not sufficient; the rigidity and stabilization provided by a neighboring layer is necessary, and one neighbor provides nearly the same amount of each, as do multiple layers.

MM was used for the stepwise compression or opening of interfaces. At each step, the outer layers were fixed after a shift of 0.01 nm. Geometry minimization of the rest of the structure was carried out before the next compression or opening step. These stepwise displacements approximate geometry changes and associated energies along reversible paths. To produce accurate descriptions of the interface geometries obtained from the MM calculations, those systems were also equilibrated at 300 K using MD until conservation of energy was established.

Electrostatic interactions were calculated using Particle Mesh Ewald sums with a nonbonded cutoff of 1 nm.⁸³ Bonds between hydrogen and heavy atoms were constrained at their equilibrium lengths using the RATTLE algorithm.⁸⁴ During the initial interface equilibrations, the positions of the carbon atoms in the functionalized graphene layers were fixed to allow the aryl-propionic groups and water molecules to approximately equilibrate. Constraints were then removed. The last 3 ns of the MD were used for the analysis of the structural features of the interfaces. Relative energy values reflect the energy required to open the equilibrated interfaces.

It should be noted that atomistic simulations were not intended to directly model the complete system probed experimentally, as a comprehensive characterization of each peeled region is beyond current computational capabilities. Rather, we have focused on intersurface hydrogen bonding in the presence of water as a major factor governing arylpropionic interfacial adhesion. In spite of the quantitative differences, the qualitative similarity in adhesion trends suggests that this mechanism predicted by simulations does contribute to experimental adhesive energy measurements.

■ ASSOCIATED CONTENT

§ Supporting Information

Details concerning the diazonium chemistry. XPS analysis of functionalized surfaces accounting for ambient water. Representative Raman spectrum. Additional information pertaining to Kendall's analysis. Details of the molecular dynamics energy profiles shown in Figure 7 in the text. Detailed discussion of UHV simulations. The Supporting Information is available free of charge on the ACS Publications website at DOI: 10.1021/acs.nanolett.5b01011.

■ AUTHOR INFORMATION

Corresponding Authors

*E-mail: espinosa@northwestern.edu.

*E-mail: g-schatz@northwestern.edu

*E-mail: stn@northwestern.edu.

Author Contributions

M.R.R., A.F., and Z.A. contributed equally to this work.

Notes

The authors declare no competing financial interest.

■ ACKNOWLEDGMENTS

This work was supported by ARO MURI Award No. W911NF-09-1-0541 and NSF Award No. CMMI-1235480. This research used resources of the QUEST cluster at Northwestern University, WestGrid, and Compute/Calcul Canada. XPS and Raman spectroscopies were carried out in the Keck-II facility of

NUANCE Center at Northwestern University. The authors are grateful to Dr. Xinqi Chen of the Keck-II facility for assistance with acquiring the Raman spectra. The authors thank Lily Mao for assistance with preparing control samples as well as Rodrigo Bernal and Rafael Soler-Crespo for helpful discussions. M.R.R. gratefully acknowledges support from the Department of Defense (DoD) through the National Defense Science and Engineering Graduate Fellowship (NDSEG) Program. M.R.R. and Z.A. gratefully acknowledge the support of the Northwestern University Ryan Fellowship and International Institute for Nanotechnology.

■ REFERENCES

- (1) Treacy, M. M. J.; Ebbesen, T. W.; Gibson, J. M. Exceptionally High Young's Modulus Observed for Individual Carbon Nanotubes. *Nature* **1996**, *381* (6584), 678–680.
- (2) Krishnan, A.; Dujardin, E.; Ebbesen, T.; Yianilos, P.; Treacy, M. M. J. Young's Modulus of Single-Walled Nanotubes. *Phys. Rev. B: Condens. Matter Mater. Phys.* **1998**, *58* (20), 14013–14019.
- (3) Yu, M.-F.; Lourie, O.; Dyer, M. J.; Moloni, K.; Kelly, T. F.; Ruoff, R. S. Strength and Breaking Mechanism of Multiwalled Carbon Nanotubes under Tensile Load. *Science* **2000**, *287* (5453), 637–640.
- (4) Peng, B.; Locascio, M.; Zapol, P.; Li, S.; Mielke, S. L.; Schatz, G. C.; Espinosa, H. D. Measurements of Near-Ultimate Strength for Multiwalled Carbon Nanotubes and Irradiation-Induced Crosslinking Improvements. *Nat. Nanotechnol.* **2008**, *3* (10), 626–631.
- (5) Lee, C.; Wei, X.; Kysar, J. W.; Hone, J. Measurement of the Elastic Properties and Intrinsic Strength of Monolayer Graphene. *Science* **2008**, *321* (5887), 385–388.
- (6) De Volder, M. F. L.; Tawfick, S. H.; Baughman, R. H.; Hart, A. J. Carbon Nanotubes: Present and Future Commercial Applications. *Science* **2013**, *339* (6119), 535–539.
- (7) Baughman, R. H.; Zakhidov, A. A.; de Heer, W. A. Carbon Nanotubes—The Route toward Applications. *Science* **2002**, *297* (5582), 787–792.
- (8) Espinosa, H. D.; Filletter, T.; Naraghi, M. Multiscale Experimental Mechanics of Hierarchical Carbon-Based Materials. *Adv. Mater.* **2012**, *24* (21), 2805–2823.
- (9) Suekane, O.; Nagataki, A.; Mori, H.; Nakayama, Y. Static Friction Force of Carbon Nanotube Surfaces. *Appl. Phys. Express* **2008**, *1* (6), 064001/1–3.
- (10) Wei, X.; Naraghi, M.; Espinosa, H. D. Optimal Length Scales Emerging from Shear Load Transfer in Natural Materials: Application to Carbon-Based Nanocomposite Design. *ACS Nano* **2012**, *6* (3), 2333–2344.
- (11) Coleman, J. N.; Khan, U.; Gun'ko, Y. K. Mechanical Reinforcement of Polymers Using Carbon Nanotubes. *Adv. Mater.* **2006**, *18* (6), 689–706.
- (12) Zhao, X.; Zhang, Q.; Chen, D.; Lu, P. Enhanced Mechanical Properties of Graphene-Based Poly(vinyl alcohol) Composites. *Macromolecules* **2010**, *43* (5), 2357–2363.
- (13) Beese, A. M.; Sarkar, S.; Nair, A.; Naraghi, M.; An, Z.; Moravsky, A.; Loutfy, R. O.; Buehler, M. J.; Nguyen, S. T.; Espinosa, H. D. Bio-Inspired Carbon Nanotube–Polymer Composite Yarns with Hydrogen Bond-Mediated Lateral Interactions. *ACS Nano* **2013**, *7* (4), 3434–3446.
- (14) Beese, A. M.; Wei, X.; Sarkar, S.; Ramachandramoorthy, R.; Roenbeck, M. R.; Moravsky, A.; Ford, M.; Yavari, F.; Keane, D. T.; Loutfy, R. O.; Nguyen, S. T.; Espinosa, H. D. Key Factors Limiting Carbon Nanotube Yarn Strength: Exploring Processing–Structure–Property Relationships. *ACS Nano* **2014**, *8* (11), 11454–11466.
- (15) Naraghi, M.; Fillette, T.; Moravsky, A.; Locascio, M.; Loutfy, R. O.; Espinosa, H. D. A Multiscale Study of High-Performance Double-Walled Nanotube–Polymer Fibers. *ACS Nano* **2010**, *4* (11), 6463–6476.
- (16) Vilatela, J. J.; Deng, L.; Kinloch, I. A.; Young, R. J.; Windle, A. H. Structure of and Stress Transfer in Fibres Spun from Carbon Nanotubes Produced by Chemical Vapour Deposition. *Carbon* **2011**, *49* (13), 4149–4158.
- (17) Balasubramanian, K.; Burghard, M. Chemically Functionalized Carbon Nanotubes. *Small* **2005**, *1* (2), 180–192.
- (18) Velasco-Santos, C.; Martínez-Hernández, A. L.; Fisher, F. T.; Ruoff, R.; Castaño, V. M. Improvement of Thermal and Mechanical Properties of Carbon Nanotube Composites through Chemical Functionalization. *Chem. Mater.* **2003**, *15* (23), 4470–4475.
- (19) Liu, L.; Barber, A. H.; Nuriel, S.; Wagner, H. D. Mechanical Properties of Functionalized Single-Walled Carbon Nanotube/Poly(vinyl alcohol) Nanocomposites. *Adv. Funct. Mater.* **2005**, *15* (6), 975–980.
- (20) Cheng, Q.; Wang, B.; Zhang, C.; Liang, Z. Functionalized Carbon-Nanotube Sheet/Bismaleimide Nanocomposites: Mechanical and Electrical Performance Beyond Carbon-Fiber Composites. *Small* **2010**, *6* (6), 763–767.
- (21) Cheng, H. K. F.; Sahoo, N. G.; Tan, Y. P.; Pan, Y.; Bao, H.; Li, L.; Chan, S. H.; Zhao, J. Poly(vinyl alcohol) Nanocomposites Filled with Poly(vinyl alcohol)-Grafted Graphene Oxide. *ACS Appl. Mater. Interfaces* **2012**, *4* (5), 2387–2394.
- (22) An, Z.; Compton, O. C.; Putz, K. W.; Brinson, L. C.; Nguyen, S. T. Bio-Inspired Borate Cross-Linking in Ultra-Stiff Graphene Oxide Thin Films. *Adv. Mater.* **2011**, *23* (33), 3842–3846.
- (23) Beese, A. M.; An, Z.; Sarkar, S.; Nathamgari, S. S. P.; Espinosa, H. D.; Nguyen, S. T. Defect-Tolerant Nanocomposites through Bio-Inspired Stiffness Modulation. *Adv. Funct. Mater.* **2014**, *24* (19), 2883–2891.
- (24) Compton, O. C.; Cranford, S. W.; Putz, K. W.; An, Z.; Brinson, L. C.; Buehler, M. J.; Nguyen, S. T. Tuning the Mechanical Properties of Graphene Oxide Paper and Its Associated Polymer Nanocomposites by Controlling Cooperative Intersheet Hydrogen Bonding. *ACS Nano* **2012**, *6* (3), 2008–2019.
- (25) Lu, W.; Zu, M.; Byun, J.-H.; Kim, B.-S.; Chou, T.-W. State of the Art of Carbon Nanotube Fibers: Opportunities and Challenges. *Adv. Mater.* **2012**, *24* (14), 1805–1833.
- (26) Espinosa, H. D.; Juster, A. L.; Latourte, F. J.; Loh, O. Y.; Gregoire, D.; Zavattieri, P. D. Tablet-Level Origin of Toughening in Abalone Shells and Translation to Synthetic Composite Materials. *Nat. Commun.* **2011**, *2* (173), 1–9.
- (27) Espinosa, H. D.; Rim, J. E.; Barthelat, F.; Buehler, M. J. Merger of Structure and Material in Nacre and Bone—Perspectives on de Novo Biomimetic Materials. *Prog. Mater. Sci.* **2009**, *54* (8), 1059–1100.
- (28) Israelachvili, J. N. *Intermolecular and Surface Forces*, 3rd ed.; Elsevier Inc.: Waltham, MA, 2011; pp 154, 278, 280–281.
- (29) Keten, S.; Xu, Z.; Ihle, B.; Buehler, M. J. Nanoconfinement Controls Stiffness, Strength, and Mechanical Toughness of β -Sheet Crystals in Silk. *Nat. Mater.* **2010**, *9* (4), 359–367.
- (30) Keten, S.; Buehler, M. J. Geometric Confinement Governs the Rupture Strength of H-bond Assemblies at a Critical Length Scale. *Nano Lett.* **2008**, *8* (2), 743–748.
- (31) Meyers, M. A.; McKittrick, J.; Chen, P.-Y. Structural Biological Materials: Critical Mechanics-Materials Connections. *Science* **2013**, *339* (6121), 773–779.
- (32) Ritchie, R. O.; Buehler, M. J.; Hansma, P. Plasticity and Toughness in Bone. *Phys. Today* **2009**, *62* (6), 41–47.
- (33) Fantner, G. E.; Hassenkam, T.; Kindt, J. H.; Weaver, J. C.; Birkedal, H.; Pechenik, L.; Cutroni, J. A.; Cidade, G. A.; Stucky, G. D.; Morse, D. E.; et al. Sacrificial Bonds and Hidden Length Dissipate Energy as Mineralized Fibrils Separate During Bone Fracture. *Nat. Mater.* **2005**, *4* (8), 612–616.
- (34) Thompson, J. B.; Kindt, J. H.; Drake, B.; Hansma, H. G.; Morse, D. E.; Hansma, P. K. Bone Indentation Recovery Time Correlates with Bond Reforming Time. *Nature* **2001**, *414* (6865), 773–776.
- (35) Farris, R. J.; Goldfarb, J. An Experimental Partitioning of the Mechanical Energy Expendited During Peel Testing. In *Adhesion Measurement of Films and Coatings*; Mittal, K. L., Ed.; Wiley: The Netherlands, 1994; pp 265–282.

- (36) Roenbeck, M. R.; Wei, X.; Beese, A. M.; Naraghi, M.; Furmanchuk, A.; Paci, J. T.; Schatz, G. C.; Espinosa, H. D. In Situ Scanning Electron Microscope Peeling To Quantify Energy between Multiwalled Carbon Nanotubes and Graphene. *ACS Nano* **2014**, *8* (1), 124–138.
- (37) Dyke, C. A.; Tour, J. M. Unbundled and Highly Functionalized Carbon Nanotubes from Aqueous Reactions. *Nano Lett.* **2003**, *3* (9), 1215–1218.
- (38) Bahr, J. L.; Tour, J. M. Highly Functionalized Carbon Nanotubes Using in Situ Generated Diazonium Compounds. *Chem. Mater.* **2001**, *13* (11), 3823–3824.
- (39) Strano, M. S.; Dyke, C. A.; Usrey, M. L.; Barone, P. W.; Allen, M. J.; Shan, H.; Kittrell, C.; Hauge, R. H.; Tour, J. M.; Smalley, R. E. Electronic Structure Control of Single-Walled Carbon Nanotube Functionalization. *Science* **2003**, *301* (5639), 1519–1522.
- (40) Lin, S.; Hilmer, A. J.; Mendenhall, J. D.; Strano, M. S.; Blankschtein, D. Molecular Perspective on Diazonium Adsorption for Controllable Functionalization of Single-Walled Carbon Nanotubes in Aqueous Surfactant Solutions. *J. Am. Chem. Soc.* **2012**, *134* (19), 8194–8204.
- (41) Hilmer, A. J.; McNicholas, T. P.; Lin, S.; Zhang, J.; Wang, Q. H.; Mendenhall, J. D.; Song, C.; Heller, D. A.; Barone, P. W.; Blankschtein, D.; et al. Role of Adsorbed Surfactant in the Reaction of Aryl Diazonium Salts with Single-Walled Carbon Nanotubes. *Langmuir* **2012**, *28* (2), 1309–1321.
- (42) Koehler, F. M.; Jacobsen, A.; Ensslin, K.; Stampfer, C.; Stark, W. J. Selective Chemical Modification of Graphene Surfaces: Distinction Between Single- and Bilayer Graphene. *Small* **2010**, *6* (10), 1125–1130.
- (43) Kirkman, P. M.; Güell, A. G.; Cuharuc, A. S.; Unwin, P. R. Spatial and Temporal Control of the Diazonium Modification of sp^2 Carbon Surfaces. *J. Am. Chem. Soc.* **2013**, *136* (1), 36–39.
- (44) Tang, Q.; Zhou, Z.; Chen, Z. Graphene-Related Nanomaterials: Tuning Properties by Functionalization. *Nanoscale* **2013**, *5* (11), 4541–4583.
- (45) Hossain, M. Z.; Walsh, M. A.; Hersam, M. C. Scanning Tunneling Microscopy, Spectroscopy, and Nanolithography of Epitaxial Graphene Chemically Modified with Aryl Moieties. *J. Am. Chem. Soc.* **2010**, *132* (43), 15399–15403.
- (46) Ma, H.; Lee, L.; Brooksbys, P. A.; Brown, S. A.; Fraser, S. J.; Gordon, K. C.; Leroux, Y. R.; Hapiot, P.; Downard, A. J. Scanning Tunneling and Atomic Force Microscopy Evidence for Covalent and Noncovalent Interactions between Aryl Films and Highly Ordered Pyrolytic Graphite. *J. Phys. Chem. C* **2014**, *118* (11), 5820–5826.
- (47) Tuinstra, F.; Koenig, J. L. Raman Spectrum of Graphite. *J. Chem. Phys.* **1970**, *53* (3), 1126–1130.
- (48) Pimenta, M. A.; Dresselhaus, G.; Dresselhaus, M. S.; Cançado, L.; Jorio, A.; Saito, R. Studying Disorder in Graphite-Based Systems by Raman Spectroscopy. *Phys. Chem. Chem. Phys.* **2007**, *9* (11), 1276–1290.
- (49) Wu, Q.; Wu, Y.; Hao, Y.; Geng, J.; Charlton, M.; Chen, S.; Ren, Y.; Ji, H.; Li, H.; Boukhvalov, D. W.; et al. Selective Surface Functionalization at Regions of High Local Curvature in Graphene. *Chem. Commun. (Cambridge, U. K.)* **2013**, *49* (7), 677–679.
- (50) Niyogi, S.; Bekyarova, E.; Itkis, M. E.; Zhang, H.; Shepperd, K.; Hicks, J.; Sprinkle, M.; Berger, C.; Lau, C. N.; Deheer, W. A.; et al. Spectroscopy of Covalently Functionalized Graphene. *Nano Lett.* **2010**, *10* (10), 4061–4066.
- (51) Huang, P.; Zhu, H.; Jing, L.; Zhao, Y.; Gao, X. Graphene Covalently Binding Aryl Groups: Conductivity Increases Rather than Decreases. *ACS Nano* **2011**, *5* (10), 7945–7949.
- (52) Fan, X.; Nouchi, R.; Tanigaki, K. Effect of Charge Puddles and Ripples on the Chemical Reactivity of Single-Layer Graphene Supported by SiO_2/Si Substrate. *J. Phys. Chem. C* **2011**, *115* (26), 12960–12964.
- (53) Dong, X.; Fu, D.; Fang, W.; Shi, Y.; Chen, P.; Li, L.-J. Doping Single-Layer Graphene with Aromatic Molecules. *Small* **2009**, *5* (12), 1422–1426.
- (54) Singh, A. K.; Iqbal, M. W.; Singh, V. K.; Iqbal, M. Z.; Lee, J. H.; Chun, S.-H.; Shin, K.; Eom, J. Molecular N-doping of Chemical Vapor Deposition Grown Graphene. *J. Mater. Chem.* **2012**, *22* (30), 15168–15174.
- (55) Kendall, K. Thin-Film Peeling—The Elastic Term. *J. Phys. D: Appl. Phys.* **1975**, *8* (13), 1449–1452.
- (56) Jorgensen, W. L.; Maxwell, D. S.; Tirado-Rives, J. Development and Testing of the OPLS All-Atom Force Field on Conformational Energetics and Properties of Organic Liquids. *J. Am. Chem. Soc.* **1996**, *118* (45), 11225–11236.
- (57) Kaminski, G. A.; Friesner, R. A.; Tirado-Rives, J.; Jorgensen, W. L. Evaluation and Reparametrization of the OPLS-AA Force Field for Proteins via Comparison with Accurate Quantum Chemical Calculations on Peptides. *J. Phys. Chem. B* **2001**, *105* (28), 6474–6487.
- (58) Ponder, J. W. *TINKER Molecular Modeling Package version 6.3*, 2015. <http://dasher.wustl.edu/tinker/> (accessed June 29, 2014).
- (59) An, Z.; Furmanchuk, A.; Ramachandramoorthy, R.; Filleter, T.; Roenbeck, M. R.; Espinosa, H. D.; Schatz, G. C.; Nguyen, S. T. Inherent Carbonaceous Impurities on Arc-Discharge Multiwalled Carbon Nanotubes and Their Implications for Nanoscale Interfaces. *Carbon* **2014**, *80*, 1–11.
- (60) Zacharia, R.; Ulbricht, H.; Hertel, T. Interlayer Cohesive Energy of Graphite from Thermal Desorption of Polyaromatic Hydrocarbons. *Phys. Rev. B: Condens. Matter Mater. Phys.* **2004**, *69* (15), 155406/1–7.
- (61) Benedict, L. X.; Chopra, N. G.; Cohen, M. L.; Zettl, A.; Louie, S. G.; Crespi, V. H. Microscopic Determination of the Interlayer Binding Energy in Graphite. *Chem. Phys. Lett.* **1998**, *286* (5), 490–496.
- (62) Girifalco, L. A.; Lad, R. A. Energy of Cohesion, Compressibility, and the Potential Energy Functions of the Graphite System. *J. Chem. Phys.* **1956**, *25* (4), 693–697.
- (63) Plaza, G. R.; Guinea, G. V.; Pérez-Rigueiro, J.; Elices, M. Thermo-Hydro-Mechanical Behavior of Spider Dragline Silk: Glassy and Rubbery States. *J. Polym. Sci., Part B: Polym. Phys.* **2006**, *44* (6), 994–999.
- (64) Wang, Y.; Porter, D.; Shao, Z. Using Solvents with Different Molecular Sizes To Investigate the Structure of *Antheraea Pernyi* Silk. *Biomacromolecules* **2013**, *14* (11), 3936–3942.
- (65) Minoshima, K.; Maekawa, Y.; Komai, K. The Influence of Vacuum on Fracture and Fatigue Behavior in a Single Aramid Fiber. *Int. J. Fatigue* **2000**, *22* (9), 757–765.
- (66) Persson, B. N. J. *Sliding Friction*, 2nd ed.; Springer-Verlag: Germany, 2000; pp 154–156.
- (67) Lebedeva, N. V.; Sun, F. C.; Lee, H.-i.; Matyjaszewski, K.; Sheiko, S. S. “Fatal Adsorption” of Brushlike Macromolecules: High Sensitivity of C–C Bond Cleavage Rates to Substrate Surface Energy. *J. Am. Chem. Soc.* **2008**, *130* (13), 4228–4229.
- (68) Blanksby, S. J.; Ellison, G. B. Bond Dissociation Energies of Organic Molecules. *Acc. Chem. Res.* **2003**, *36* (4), 255–263.
- (69) Drummond, C. J.; Chan, D. Y. Van der Waals Interaction, Surface Free Energies, and Contact Angles: Dispersive Polymers and Liquids. *Langmuir* **1997**, *13* (14), 3890–3895.
- (70) Wawra, H. Surface Energy of Solid Materials As Measured by Ultrasonic and Conventional Test Methods. Part 1. *Zeitschrift Fur Metallkunde* **1975**, *66* (7–8), 395–401, , 492–498.
- (71) Ge, L.; Sethi, S.; Ci, L.; Ajayan, P. M.; Dhinojwala, A. Carbon Nanotube-Based Synthetic Gecko Tapes. *Proc. Natl. Acad. Sci. U. S. A.* **2007**, *104* (26), 10792–10795.
- (72) Paci, J. T.; Furmanchuk, A.; Espinosa, H. D.; Schatz, G. C. Shear and Friction Between Carbon Nanotubes in Bundles and Yarns. *Nano Lett.* **2014**, *14* (11), 6138–6147.
- (73) Na, S. R.; Suk, J. W.; Tao, L.; Akinwande, D.; Ruoff, R. S.; Huang, R.; Liechti, K. M. Selective Mechanical Transfer of Graphene from Seed Copper Foil Using Rate Effects. *ACS Nano* **2015**, *9* (2), 1325–1335.
- (74) Na, S. R.; Suk, J. W.; Ruoff, R. S.; Huang, R.; Liechti, K. M. Ultra Long-Range Interactions between Large Area Graphene and Silicon. *ACS Nano* **2014**, *8* (11), 11234–11242.

- (75) Yang, Y.; Xu, Z.-H.; Pan, Z.; Li, X. Hydrogen Passivation Induced Dispersion of Multiwalled Carbon Nanotubes. *Adv. Mater.* **2012**, *24* (7), 881–885.
- (76) Yang, Y.; Rigdon, W.; Huang, X.; Li, X. Enhancing Graphene Reinforcing Potential in Composite by Hydrogen Passivation Induced Dispersion. *Sci. Rep.* **2013**, *3* (2086), 1–7.
- (77) Wei, X.; Filleter, T.; Espinosa, H. D. Statistical Shear Lag Model—Unraveling the Size Effect in Hierarchical Composites. *Acta Biomater.* **2015**, *18*, 206–212.
- (78) Yuzvinsky, T. D.; Fennimore, A. M.; Mickelson, W.; Esquivias, C.; Zettl, A. Precision Cutting of Nanotubes with a Low-Energy Electron Beam. *Appl. Phys. Lett.* **2005**, *86* (S), 053109/1-3.
- (79) Caleman, C.; van Maaren, P. J.; Hong, M.; Hub, J. S.; Costa, L. T.; van der Spoel, D. Force Field Benchmark of Organic Liquids: Density, Enthalpy of Vaporization, Heat Capacities, Surface Tension, Isothermal Compressibility, Volumetric Expansion Coefficient, and Dielectric Constant. *J. Chem. Theory Comput.* **2012**, *8* (1), 61–74.
- (80) Zubillaga, R. A.; Labastida, A.; Cruz, B.; Martínez, J. C.; Sánchez, E.; Alejandre, J. Surface Tension of Organic Liquids Using the OPLS/AA Force Field. *J. Chem. Theory Comput.* **2013**, *9* (3), 1611–1615.
- (81) Hub, J. S.; Caleman, C.; van der Spoel, D. Organic Molecules on the Surface of Water Droplets – an Energetic Perspective. *Phys. Chem. Chem. Phys.* **2012**, *14* (27), 9537–9545.
- (82) Berendsen, H.; Postma, J.; Van Gunsteren, W.; Hermans, J. Interaction Models for Water in Relation to Protein Hydration. In *Intermolecular Forces, The Jerusalem Symposia on Quantum Chemistry and Biochemistry*; Pullman, B., Ed.; D. Reidel Publishing Company: Dordrecht, Holland, 1981; pp 331–342.
- (83) Essmann, U.; Perera, L.; Berkowitz, M. L.; Darden, T.; Lee, H.; Pedersen, L. G. A Smooth Particle Mesh Ewald Method. *J. Chem. Phys.* **1995**, *103* (19), 8577–8593.
- (84) Andersen, H. C. RATTLE: A “Velocity” Version of the SHAKE Algorithm for Molecular Dynamics Calculations. *J. Comput. Phys.* **1983**, *52* (1), 24–34.